# Experimental analysis of CFRP laminates subjected to Compression After Impact: the role of impact-induced cracks in failure

Samuel Rivallant, Christophe Bouvet, Elias Abi Abdallah, Bernhard Broll, Jean-Jacques Barrau

# Experimental analysis of CFRP laminates subjected to compression after impact: The role of impact-induced cracks in failure

Samuel Rivallant *, Christophe Bouvet, Elias Abi Abdallah, Bernhard Broll, Jean-Jacques Barrau

*Université de Toulouse; INSA, UPS, Mines Albi, ISAE; ICA (Institut Clément Ader), 10 avenue Edouard Belin, BP54032, 31055 Toulouse Cedex 4, France*

ARTICLE INFO

*Keywords:*
Composite laminates
Low velocity impact
Damage tolerance
Crack propagation
Digital image correlation

ABSTRACT

This paper presents an experimental analysis of composite laminates subjected to low velocity impact and compression after impact (CAI). Two types of CFRP specimens are studied: a highly oriented laminate and a quasi-isotropic laminate. Impact energy is chosen to obtain a dent depth less than or around the BVID level. 3D digital image correlation is used to make detailed analyses of plates behaviour during CAI. Even if the damage morphologies are very different, the study shows that, in both cases, classical global buckling of the plate and local buckling of the delaminated sublaminates are accompanied by a crack on the impact face of the laminate. This crack appears in the highly damaged zone, under the impactor, and propagates in the direction transverse to the loading direction in a stable way. It is shown to play an essential role in the final failure of the laminate under compression.

## 1. Introduction

A limitation in the use of composites in structural design, especially in the field of aeronautics, is its low impact resistance. In fact, subjected to low-velocity/low-energy impact as during maintenance or even in production line, a structure – even with apparently minor damage – may suffer a sever decrease in mechanical strength, especially for compression loading. That is why the concept of damage tolerance was introduced. An aeronautical composite structure is allowed to fly if it can be shown that, despite the presence of damage in the material – even invisible on the surface – the structure can sustain the loads [1]. To do this, CAI (compression after impact) tests are usually performed, as compression is generally the most critical case for dimensioning of structures that have already been subjected to impact. A large number of studies concerning impact on composite structures, especially on CFRP laminates, is available in the literature. Paradoxically, there is much less research on CAI, while the ultimate objective of manufacturers is precisely to know the residual strength of structures.

In recent years, studies on CAI have largely focused on modelling the residual strength with analytical [2,3], semi-empirical [4], or finite elements [5–10] approaches, even though the physical mechanisms leading to the final rupture are still not well known today. Indeed, among the experimental studies, some focus on the influence of material properties on the evolution of the residual strength: fibre [8,11], resin [11–13], interface [14], stacking [15], transverse reinforcement like stitching [16,17] or Z-pinning [18], fabric instead of unidirectional tape [12,19], curing temperature [19]. There are also some experimental studies concerning the influence of test conditions such as: temperature during impact [20], hygrothermal conditions [12,21–23], fatigue loading [24], or use of protective layer [25]. However, the vast majority of these studies does not focus on a detailed understanding of damage mechanisms leading to the final rupture in CAI, but only on the level of residual strength.

Nevertheless, there are some works dealing with these aspects. A number of studies shows that during CAI, damage created by the impact provokes, under compression, local buckling of the sublaminates in the area of the impact, forming a blister. Sometimes, it is even possible to observe the propagation of delamination due to this buckling [13,18,26,27]. The majority of researchers agree that, indeed, the buckling (especially local buckling) plays a key role in the final rupture [13,15,18,25–31]. However, this phenomenon is not sufficient to explain the final failure of the structure, since in most cases the delamination does not propagate over the entire width of the plate, and the final rupture is due to the sudden propagation of a crack from the impact zone to the edges of the structure.

Some authors assume that the onset of the final failure is likely due to local compression failure at the edge of the damage [22,32,33], but without significant proof. Kinsey et al. [19] show with X-ray techniques that in carbon fabrics, during CAI, some cracks appear before 80% of the final failure load, grow in a stable manner, and then suddenly propagate in the whole plate, leading

* Corresponding author. Tel.: +33 (0)5 61 33 81 58.
*E-mail addresses:* samuel.rivallant@isae.fr (S. Rivallant), christophe.bouvet@isae.fr (C. Bouvet).

to the final rupture. They also assume that these cracks are due to microbuckling of fibres in the 0° plies. Using glass fibre UD laminates, Aktas et al. [20] also show the presence and the propagation of such cracks during CAI. But again, this study does not permit to define the nature of this crack, and its origin: fibre failure in compression, or fibre failure due to bending when buckling occurs. Yan et al. [8] present the same kind of cracks in glass fabrics, where cracks and delamination propagate together. Post-mortem observations lead him to conclude that they are shear cracks. Uda et al. [24] show that, during CAI tests under fatigue loading on UD AS4/PEEK carbon laminates, cracks appear and propagate in the 0° plies: SEM observations clearly show the presence of kink bands due to compression in these cracks. Soutis and Curtis [34] also talk about the development of kink bands in the vicinity of the damaged area under impact, which is in fact the assumption that allows them to compare the behaviour of impacted laminates in CAI to the one of laminates with open hole, in order to define their model for prediction of residual strength. Finally, more recently, Aymerich and Priolo [16] clearly demonstrate the presence of crack paths due to fibre failure in 0° plies, for laminates with transverse reinforcements (stitching).

In summary, it is known that existing damage due to impact can lead to local buckling of sublaminates during a posterior CAI test, with or without propagation of delamination, provided that the impact energy level is not too low. Buckling may also be accompanied by fibre failure cracks, especially in the 0° plies, which can grow stably, usually in the direction transverse to the loading direction. However, there is still much debate on the final collapse of plates in CAI. The final rupture is obtained by propagation of a macro-crack from the impact zone towards the edges of CAI specimens. But the question is still open regarding the initiation of this crack around the impact zone (buckling, fibre failure cracks etc.), the nature of this crack (compression, shear, mixed mode), and the transition from an eventual stable damage propagation to the sudden final rupture.

This paper focuses on CAI tests performed on two different types of plates, but all coming from problematics linked to the aeronautical industry. The first type is a highly oriented composite laminate that can be used, for example, in compression beams. It leads to a specific morphology of impact damage. The second one is a more classical quasi-isotropic laminate with relatively well-known impact damage. The objective is to obtain a more detailed identification of the mechanisms leading to the final failure in compression of these two different types of plates that were first impacted. Moreover, the interest in testing a highly oriented laminate, with ply clustering, is also to draw a parallel between what happens in oriented and classical laminates, as it is easier to observe and analyse failure mechanisms in the first case. In practice, a detailed analysis is performed, from multi-instrumented CAI tests. Special attention is given to the role of initial damage on the onset of buckling and development of cracks.

A fine understanding of the mechanisms that trigger the final collapse is essential, as it would allow to propose new criteria for rupture prediction in CAI simulation, and then improve residual strength calculation and more generally the design of composite laminates according to the damage tolerance concept.

## 2. Materials

Two different CFRP laminates were used in this study. The first one is a highly oriented laminate (specimen HO) made by RTM process. The second one is a quasi-isotropic laminate (specimen QI) made of UD prepregs.

HO specimens are 12 layers plates made of G30-500 GK HTA-76 carbon fibre infused with RTM6 epoxy resin. Two different layers were used to stack these laminates. One of these layers is a nearly balanced 0.2 mm thick woven fabric and the other one is a 0.3 mm thick quasi-UD ply. A woven fabric layer is placed on each face where 10 quasi-UD are put between them. All these quasi-UD layers are oriented along the 0° direction.

**Table 1**
G30-500/RTM6 and T700/M21 material properties.

| | G30-500/RTM6 Woven fabric | G30-500/RTM6 Quasi-UD | T700 /M21 UD |
|---|---|---|---|
| $E_l^t$ (GPa) | 60 | 108 | 130 |
| $E_t^t$ (GPa) | 55 | 8 | 7.7 |
| $E_l^c$ (GPa) | 47 | 87 | 100 |
| $E_t^c$ (GPa) | 49 | 8 | 7.7 |
| $G_{lt}$ (GPa) | 3.15 | 2.94 | 4.8 |
| $\nu_{lt}$ | 0.07 | 0.3 | 0.3 |
| $\sigma_t^t$ (MPa) | 639 | 52 | 60 |
| $\sigma_t^c$ (MPa) | −480 | −228 | *n/a* |
| $\tau_{lt}$ (MPa) | 64 | 94 | 110 |
| $\varepsilon_l^t$ (μstrain) | 13,200 | 13,000 | 16,000 |
| $\varepsilon_l^c$ (μstrain) | −12,150 | −10,150 | −12,500 |

QI specimens are made of 0.26 mm thick T700/M21 unidirectional carbon/epoxy plies, with stacking sequence $[02, 452, 902, -452]_{sym}$, for a total thickness of 4.16 mm.

The mechanical properties of each material are evaluated experimentally or taken from the literature. They are listed in Table 1, where $E_l^t(E_t^t)$ and $E_l^c(E_t^c)$ are the young modulus in tension and compression in the fibres (transverse) directions, $G_{lt}$ and $\upsilon_{lt}$ are the shear modulus and the Poisson's ratio in the l–t plane, $\sigma_t^t$ and $\sigma_t^c$ are the failure stresses in tension and compression in the transverse direction, $\varepsilon_l^t$ and $\varepsilon_l^c$ are the failure strains in tension and compression along the fibre directions, and $\tau_{lt}$ is the failure shear stress.

## 3. Low velocity impact and static indentation tests

For both materials, laminates were cut into $150 \times 100\ mm^2$ plates and impacted at the centre. Impact tests were performed with a drop tower, with 0–30 J energy levels approximately. The impactor was a 2 kg rigid mass with a 16 mm diameter hemispherical tip, according to Airbus Industries Test Method (AITM 1-0010) [35]. Additional static indentation tests were also performed on a universal tension/compression testing machine at a constant speed, using the same hemispherical tip. QI specimens were simply supported on a $75 \times 125\ mm^2$ window (dot-line in Fig. 2). The specificity of the HO plates stacking sequence led to adapt the boundary conditions. HO specimen were clamped along the length and left free along the width: the working part of the plate during the tests is $42 \times 150\ mm^2$, as illustrated on Fig. 1a (more details available in [36]). Besides, to study the influence of the damage on the compressive residual strength, tests were performed at different levels of energy or maximum displacement. Details of tests performed before CAI tests are available in Tables 2 and 3, where $E$ ($J$) is the energy supplied during the test, $d_{max}$ (mm) is the maximum displacement reached during the test (imposed displacement for static tests), $F_{max}$ is the maximum force, and $I_{perm}$ the permanent indentation 48 h after the test. For both static and dynamic tests, the energy is calculated from experimental data as the integral of force with respect to displacement, from 0 to the maximum displacement. It is not only the energy dissipated by damage, but the maximum energy supplied during the test.

### 3.1. Damage in highly oriented plates

The purpose of the present paper is to analyse the effect of impact damage on the CAI strength. Details of impact results on such

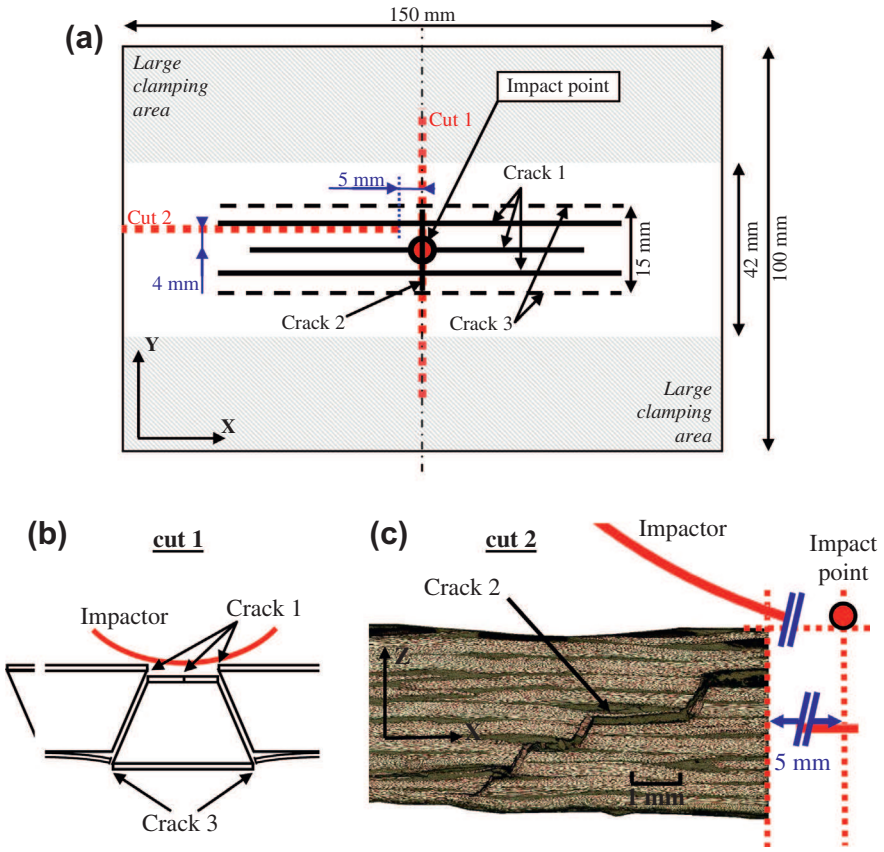


**Fig. 1.** Main damage after impact in HO plates: (a) localisation of main cracks, (b) trapezoidal shaped damage, and (c) crack 2.

**Table 2**
HO plates – impact and static indentation: configurations and main results.

| Kind of test | $E$ | $d_{max}$ | $F_{max}$ | $I_{perm}$ |
|---|---|---|---|---|
| Undamaged | – | – | – | – |
| Impact | 14 | 4.2 | 4.6 | 0.37 |
| | 18.5 | 5.0 | 5.3 | 0.65 |
| | 23 | 6.0 | 5.1 | 1.05 |
| Static | 12.5 | 4.2 | 4.5 | 0.60 |
| | 16 | 5.0 | 4.6 | 1.05 |
| | 21 | 6.2 | 4.5 | 1.30 |

highly oriented laminates have been previously presented in [36], thus only the necessary data will be presented here.

Due to its specific stacking sequence, damage inside HO plates is very particular (Fig. 1). Chronologically, 45° microcracks appear in the quasi-UD on the back face of the laminates under the impactor, and propagate in the thickness till the impact face, and then along the lower fabric, to induce delamination. Next step is the rupture of the upper fabric (cracks 1), and afterward, rupture of the lower fabric (cracks 3), that both propagate then in the longitudinal direction ($x$). At this moment, the damage consists mostly in a partially detached stripe with a trapezoidal section. In parallel, a crack (crack 2) appears and propagates in the transverse direction ($y$). This crack is of first importance, as it plays a major role in the final rupture of the laminate in CAI (see Section 4). The comparison between static and dynamic tests shows similarities in quantity and form in the damage except for the permanent indentation, which is higher in the static cases.

**Table 3**
QI plates – impact and static indentation: configurations and main results.

| Kind of test | $E$ | $d_{max}$ | $F_{max}$ | $I_{perm}$ |
|---|---|---|---|---|
| Impact | 1.6 | 1.2 | 2.3 | 0 |
| | 6.5 | 2.5 | 4.5 | 0.06 |
| | 17 | 4 | 6.7 | 0.23 |
| | 26.5 | 5.5 | 7.6 | 0.52 |
| | 29.5 | 5.9 | 8 | 0.70 |
| Static | 5.5 | 2.5 | 4.2 | 0.12 |
| | 17 | 4.5 | 7.9 | 0.34 |
| | 23.9 | 5.3 | 9.28 | 0.48 |

### 3.2. Damage in quasi-isotropic plates

The damage in QI specimen is more classical, with the well-known helix-shape delamination increasing in the depth of the plate. This damage is also increasing with the impact energy level. Fig. 2 shows C-Scans of 6.5 J and 29.5 J impact tests, which reveal delamination areas inside the plate.

In terms of damage, delamination is accompanied by fibre failure and intralaminar matrix cracking. All these types of damage result in a visible mark left onto the impact face of the plate: the permanent indentation. Values of the permanent indentation, measured 48 h after the impact, are given in Table 3.

## 4. Compression after impact tests

CAI tests were done on damaged and undamaged plates in order to determine the influence of damage on the compressive residual strength.

### 4.1. CAI test set-up

CAI tests were also performed according to the AITM 1-0010 standards [35] (Fig. 3), with an adaptation for HO specimen: due to their high flexibility, the distance between stabilizing knifes-edges was decreased to 75 mm instead of the 90 mm used for the QI plates (Fig. 4), which was enough to obtain a stable propagation of cracks due to fibres failure in compression.

Tests were conducted in a compression testing machine at a 0.2 mm/min imposed speed. Plates and instrumentation are presented in Fig. 4.

A LVDT sensor was used to measure the displacement imposed by the machine, in the loading direction. A second LVDT sensor was set at the centre of the back face of the plate to measure the out-of-plane displacement. In addition to these sensors, two strain gages were bonded on the back face of the plate in order to verify the loading of the specimen, and analyse the buckling. The average of these two strains is called $\varepsilon_{gages}$.

Furthermore, the impact face of the plate was monitored by a 3D Digital Image Correlation system made of two CCD cameras pointing to the central area of the plate. These cameras are used to measure the out-of-plane displacement of the impacted zone and analyse the strain distribution. Two virtual strain gages are also defined from the DIC: they are located at the same place than the strain gages, but on the opposite face of the plate (impact face). $\varepsilon_{CCD}$ is defined as the average of these two virtual strains.

Then compression ($\varepsilon_{compression}$) and bending ($\varepsilon_{bending}$) strains are defined to analyse the global buckling of the plates (Eqs. (1) and (2)).

$$\varepsilon_{compression} = \frac{\varepsilon_{CCD} + \varepsilon_{gages}}{2} \quad (1)$$

$$\varepsilon_{bending} = \frac{\varepsilon_{CCD} - \varepsilon_{gages}}{2} \quad (2)$$

### 4.2. CAI on highly oriented plates: results and discussion

#### 4.2.1. Global results

Fig. 5 shows the mean stress curve in the specimen as a function of the imposed displacement for two HO plate cases: the non-impacted test and the 23 J impact test. All the tests give similar curves. We note on these curves the presence of two phases. The first one, linear, corresponds to the increase of stress when the plate is subjected to compression loading. The slope of this curve is the same for healthy and damaged samples: the presence of initial damage has little influence on the plate membrane stiffness. The second part corresponds to the appearance of an overall buckling of the plate, and the damage propagation in the plate. So the knee-point refers to the beginning of buckling.

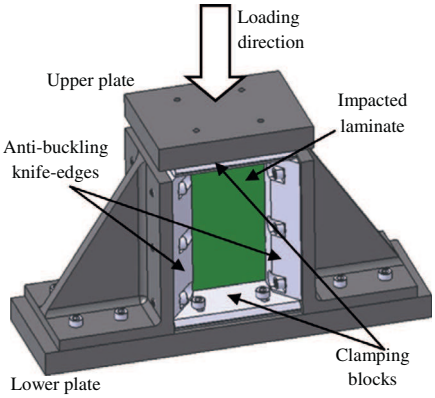


**Fig. 3.** CAI setup.

Fig. 6 shows the evolution of the failure stress and the buckling stress (see following section for details on the calculation of buckling stress). There is a significant decrease in failure stress, up to 30%, with increasing impact energy. There are few differences between dynamic tests and quasi-static tests. In any case, the small number of tests does not give a significant trend in this respect.

Non-impacted specimen breaks at one extremity of the plate, while all the damaged plates break at the centre.

#### 4.2.2. Buckling

To analyse the global buckling of plates, data from out-of-plane displacement, back face gages, and virtual gages from correlation fields are used (see Fig. 7).

The buckling stresses are determined from the first nonlinearities on the curves of out-of-plane displacement or gages. They are indicated by the dashed rectangle in Fig. 7, and presented for all tests in Fig. 6. Note that $\varepsilon_{compression}$ curve, which should be linear even after buckling, because compression stiffness is independent from bending, shows a non-linearity due to the fact that gages and virtual gages are unfortunately not located exactly at the same place, due to technical constraints during testing.

Despite the modifications in CAI test set-up, global buckling appears early in the test, and Fig. 6 shows that the buckling stress decreases significantly with increasing initial damage. For all tests, the out-of-plane displacement due to global buckling is in the same direction, and keeps increasing till failure. However, CAI strength remains significantly higher than buckling stress (Fig. 6).

The buckling is also analysed thanks to the CCD cameras and the associated cartographies of the out-of-plane displacement around the impact point. Cuts parallel to *Y* axis and passing by the centre of the plate at different compressive loadings lead to the out-of-plane curves in Fig. 8 for the 23 J impacted plate case.

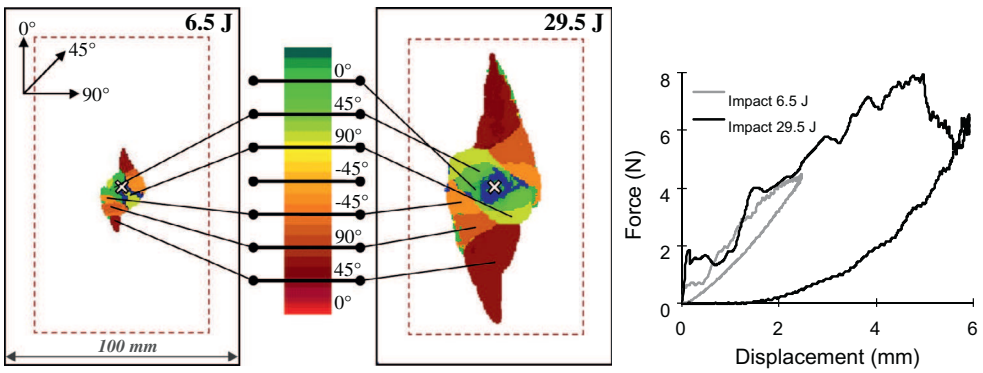


**Fig. 2.** QI plate C-Scan and force/displacement curve: 6.5 J and 29.5 J impact.

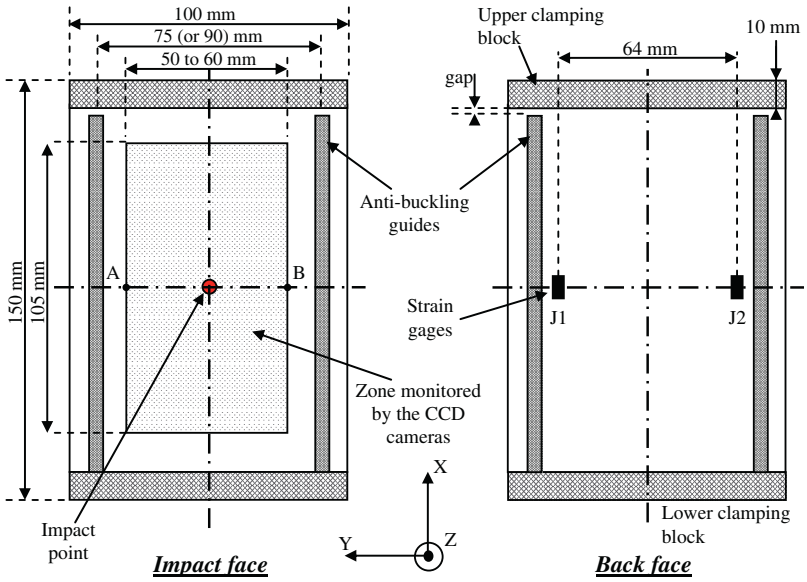


**Fig. 4.** Instrumented laminate for CAI test.

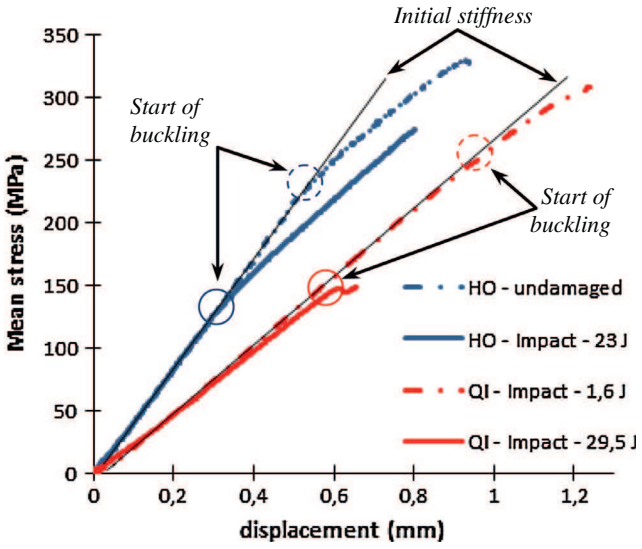


**Fig. 5.** Example of mean stress/In-plane displacement curves during CAI for HO and QI plates.

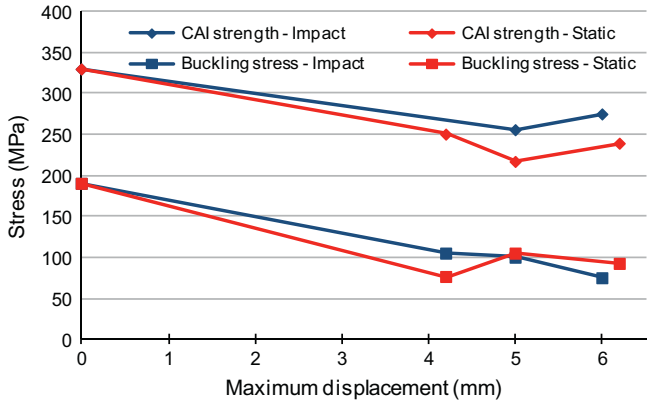


**Fig. 6.** Evolution of CAI strength and buckling stress in function of the maximum displacement reached during impact or static tests for HO plates.

These curves show the evolution of the global shape of the plate during CAI, and especially the global buckling of the plate, and the local buckling of the partially detached central part.

*4.2.3. Crack 2 propagation and final failure*

Another thing to be monitored during the compression after impact test is the evolution of crack 2. The detection of this crack and its evolution are done with the CCD cameras. Different cuts parallel to the *X*-axis are done and the displacement *u* (in *X* direction) is measured (Fig. 9). When there is no failure along that cut, the *u* curve is approximately smooth. However, the existence of a discontinuity means that the upper part moves down more than the lower part which gives an indication of a discontinuity between the two parts. This phenomenon can be explained by the presence of crack 2. Fig. 9 presents an example of two *u* curves with different cut locations *y*. A discontinuity can clearly be seen in the curve of cut 2. By minimising the distance between the different cuts, the tips of crack 2 can be localized and the length of this crack can be calculated. The same method was tested on out-of-plane displacement curves but discontinuities are less obvious.

The initial length of crack 2 only depends on the impact or indentation maximum displacement. In different terms, when the displacement of the impactor is increased, the length of the crack 2 is higher.

Fig. 10 shows the evolution of crack 2 length as a function of the applied stress until the total failure of the specimen during four CAI tests. It can be remarked that the length of this crack remains constant (no propagation) until a certain stress which is far greater than the buckling stress. Afterwards the crack starts to propagate smoothly while out-of-plane displacement increases, before leading to the total failure of the specimen. The domain of stable growth of the crack can be significant, as the length before instability can be more than twice the initial length. The evolution of the crack can be explained by looking at the stress and strain fields around the crack tip. Indeed, the propagation of the crack 2 as a function of the strain through *x* axis is plotted in Fig. 11. The strain is determined at the crack tip from the CCD cameras by computing the partial derivatives of the displacement field. It must be noted that when the crack 2 propagates, the location *y* where the strain is calculated also changes. It can be seen that the length of this

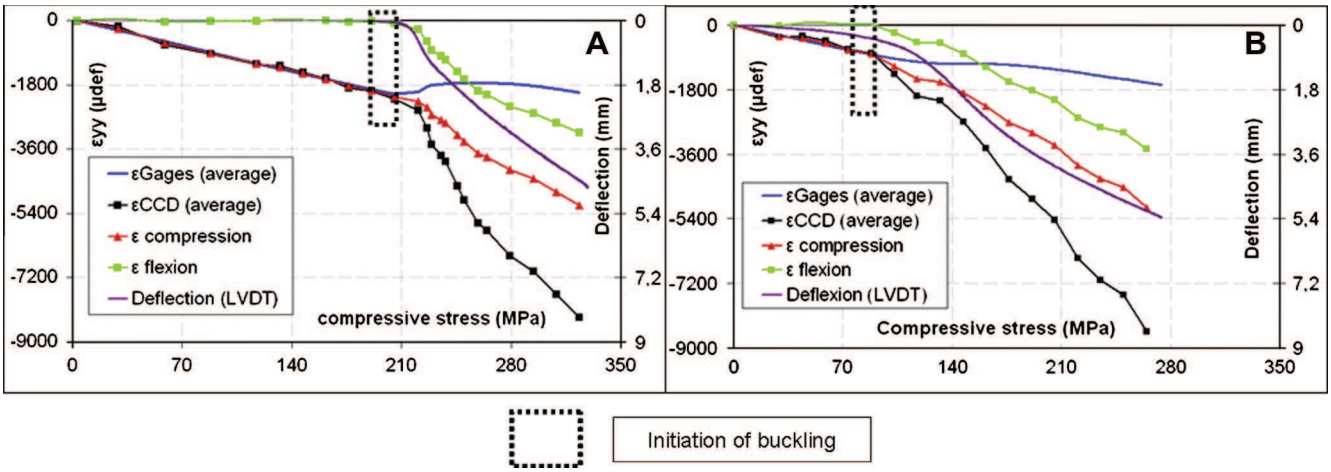


**Fig. 7.** Gages and DIC results of CAI tests: (A) non-impacted HO plate and (B) HO plate impacted at 23 J.

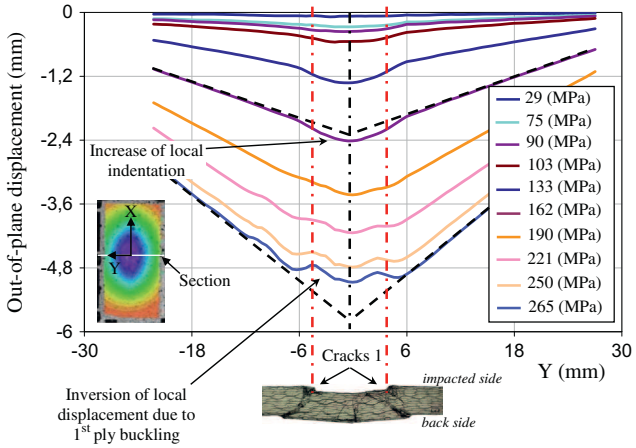


**Fig. 8.** Out-of-plane displacement during CAI for the 23 J impacted HO plate (impact face).

crack remains constant until a strain varying between 7000 and 11,000 µdef, and starts to propagate and reaches its maximal length at a strain of about 12,000 and 13,000 µdef coming along with the total failure of the specimen. These strain values are close to the failure strains of the materials (woven fabric and quasi-UD). It means that the crack propagates only if the failure strain is reached in the fibres at the tip of the crack.

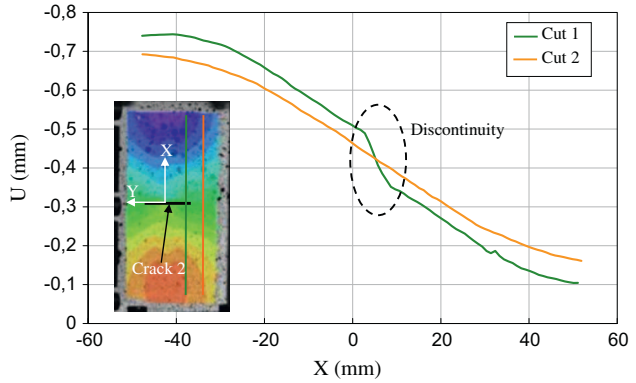


**Fig. 9.** Method for determination of crack 2 tip.

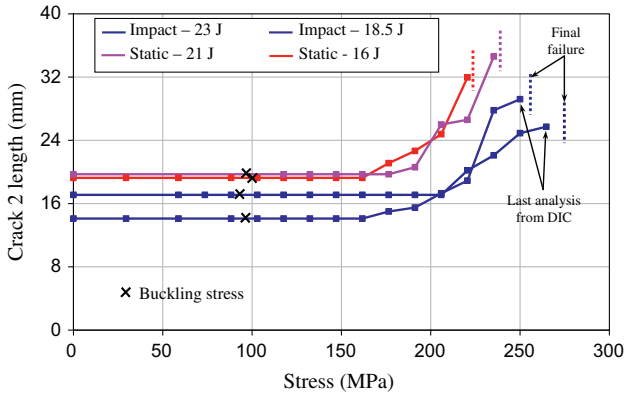


**Fig. 10.** Evolution of crack 2 length in function of stress during CAI for HO plates.

One must remain cautious regarding the quantitative values obtained by this method because the measurement accuracy is difficult to assess and the region chosen to derive the displacement field - and thus get these strain calculation – have a significant influence on these values especially in areas of high gradient deformation. Moreover, as the reference image for DIC is the image taken at the beginning of CAI test, the field calculated by DIC does not take into account the real strains: all strains are equal to zero after impact, and only the additional strains due to CAI are calculated.

To sum up: after buckling, compressive stresses and strains in the fibre direction, around the crack 2 tip, increase with the out-of-plane displacement. When strains reach a level close to the failure strain, the crack starts to propagate due to fibre failure in compression. As the out-of-plane displacement still increases with the applied load, the crack grows, which means that the crack propagation is ruled by the global buckling. The third step of CAI test is when the crack becomes unstable and suddenly leads to the overall plate failure: the final failure is then due to an instability problem, linked to the shape of the buckled plate, but above all to the presence of the initial post-impact crack. Without this crack, the plate would sustain superior loads.

### *4.3. CAI on quasi-isotropic plates: results and discussion*

In the light of the results obtained on HO plates, the same kind of analyses were made on the more classical QI plates, to see

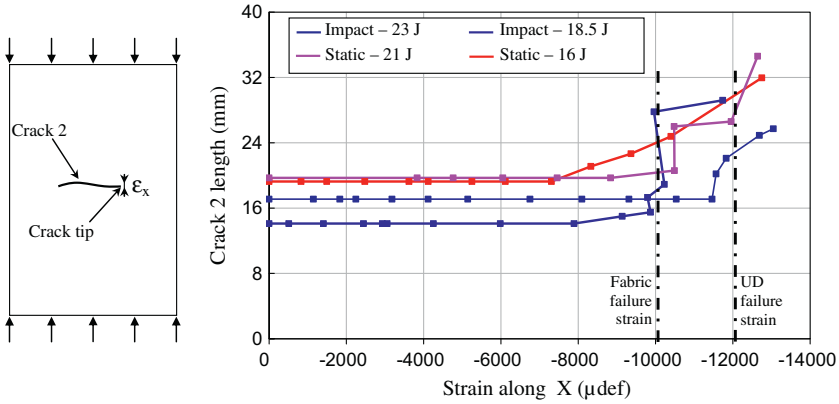


**Fig. 11.** Evolution of crack 2 length in function of the compressive strain in *X* direction at crack tip for HO plates.

whether the presence of cracks can play a role in the failure process.

*4.3.1. Global results*

CAI tests were carried out on the impact configurations presented in Table 3. Fig. 5 shows the mean stress curve in the specimens as a function of the imposed displacement for two of those configurations (1.6 J and 29.5 J). All tests result in similar curves. The nonlinearities just before rupture are not as pronounced as in the HO plates because buckling occurs at loads closer to failure.

Fig. 12 presents the evolution of CAI stress with the impact (or static indentation) energy and permanent indentation (measured 48 h after the impact tests). The decrease in strength due to impact is also greater than 30% for impact at more than 25 J. All the damaged plates break at the centre except the 1.6 J impact test, for which rupture occurs at one extremity of the plate, and the 6.5 J impact test, for which failure occurs at the third of the plate. The case of 17 J impact is specific, as buckling appeared in the opposite direction compared to what is commonly obtained.

*4.3.2. Buckling*

Fig. 13 shows the out-of-plane displacement at the centre of the plate versus the stress during three different CAI tests. The more damaged is the plate after impact (or static indentation) the faster is the increase of out-of-plane displacement during CAI. To see if this displacement is due to local or global buckling, a more precise analysis of the 29.5 J impact case was done using gages, DIC from CCD cameras and LVDT sensors. Fig. 14 shows the three classical steps: first, a quite homogeneous compression of the overall plate, till point A. Then, a slight increase of the plate thickness (difference between displacement at back face and impact face) can be observed between points A and B. It is due to the local buckling of sublaminates around the impact point. Finally, the plate suddenly

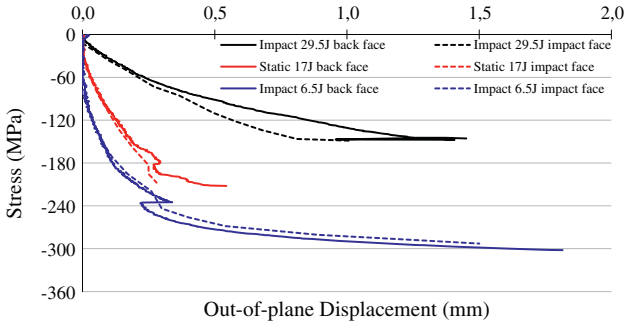


**Fig. 13.** Stress/out-of-plane displacement curve during CAI for three QI plates.

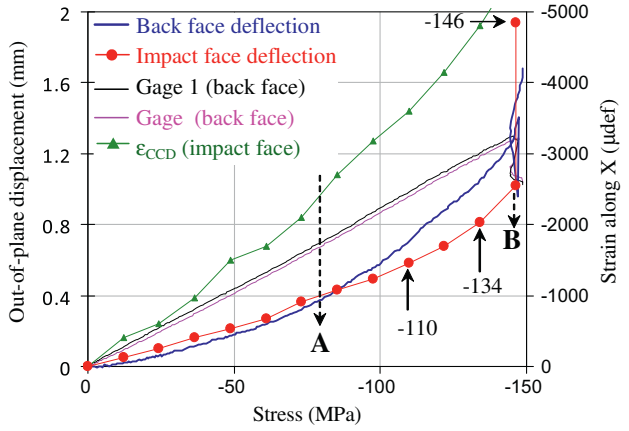


**Fig. 14.** (a) Out-of-plane displacement and strain gages curves during CAI −29.5 J impact QI plate.

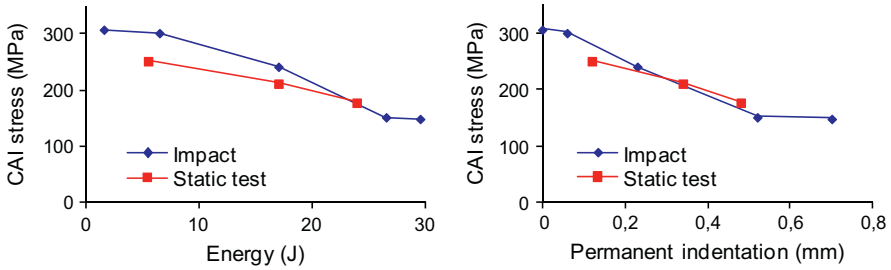


**Fig. 12.** CAI strength versus impact energy (a) and permanent indentation (b) for QI plates.

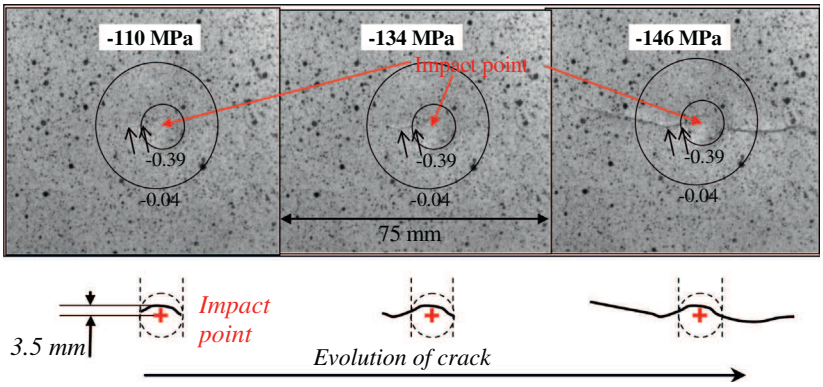


**Fig. 15.** Pictures of cracks during CAI: 29.5 J impact QI plate.

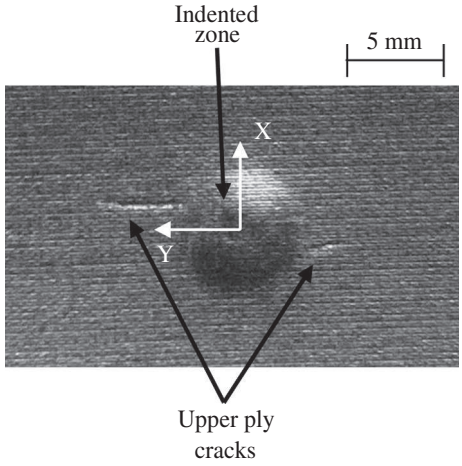


**Fig. 16.** Post-impact cracks: 27.3 J static indentation test on QI plate.

fails. No global buckling of the plate occurs, as proved by the linearity of gages curves till the failure.

*4.3.3. Crack propagation and final failure*

As for HO plates, DIC analysis of the 29.5 J impact shows the creation of a crack in the impact zone and its propagation during CAI tests. Once again, the best way to follow the crack is to look at the longitudinal displacement ($x$), which seems to be the more relevant parameter for that kind of crack.

Fig. 15 shows pictures of the impact face taken during the CAI test made after a 29.5 J impact. Until −110 MPa, the crack is not clearly visible, as it is confined in the vicinity of the impact mark, and remains hidden by the paint. When the crack propagates in the upper ply, it also propagates in the paint, and then is clearly visible. Fig. 16 presents the photo of the cracks induced by a 27.3 J static indentation before painting, which proves the presence of these post-impact cracks in some of the impacted (or indented) laminates before any CAI loading. However, they are not so obvious on all the specimen tested.

In Fig. 17, out-of-plane displacement and longitudinal strain fields obtained from DIC are represented. Iso-lines for −0.04 and −0.39 mm of initial out-of-plane displacement (measured after impact) are also drawn to give an idea of the post-impact indentation. The first delaminated interface and the crack obtained at final CAI failure are also presented. It is seen in these photos that when the CAI stress reaches about −110 MPa, a crack start to propagate from the strongly damaged zone, and especially from the middle of the area highly indented by the impact. This crack is easily observable through the deformation field $\varepsilon_{xx}$ determined by DIC, and only takes place in the upper plies (no crack on the back face). It should be noted that the value of minimum deformation chosen for scale is the compressive deformation of the material and thus a higher deformation in absolute value would inevitably lead to material failure. The same comments as for HO plates can be made regarding the limitations in strain calculation from DIC in this kind of test.

To complete this analysis, a more specific study of the crack was led on all CAI tests where a crack appeared: impact at 26.5 J and 29.5 J, and static tests at 17 J and 23.9 J. Fig. 18 shows the evolution of crack length with the applied stress. The definition of crack length is the distance between the two extremities of the crack. More precisely, Fig. 19 presents the position of the crack tips (left and right). These curves clearly show that for these four different test cases, a crack appears during CAI and propagates during the test. For the 26.5 J and 29.5 J impact, the crack appears early in the test and has a stable propagation. In the cases of 17 J and 23.9 J static tests, the crack appears lately. Fig. 19 clearly shows that the crack initiates inside the highly indented area around the impact (or indentation) point, i.e. within an 8 mm radius area approximately, and more precisely, at 3.5–4 mm from the centre of the impact zone (see Fig. 15). Only the crack in the 29.5 J impact case propagates outside this zone in a stable way. It must be noted that the location of the cracks tips and thus the value of crack length when the compressive load is low must be treated with caution. Indeed, with the method used to detect the crack (Fig. 9), it is necessary to have a differential displacement in $x$ direction between the two sides of the crack, and unfortunately, for low loads, this displacement is very small. This is the reason why these values are hidden in Fig. 19 (hatched area).

To understand the presence of this crack and the reason for its initiation at that location (i.e. inside the highly indented area), microscopic observations were made on a specific specimen. Fig. 20 shows a microscope image of a section of the 24.8 J statically indented plate (5.4 mm of maximum displacement). The cut was made in the $y$ direction. A crack can clearly be seen in the upper 45° double-ply and in the external 0° ply. Its location appears to correspond to the location found for the initiation of crack studied in the CAI tests. This proves that, even if not easily detectable from a single observation, a post-impact crack exists in the upper plies of the laminate, under the impactor.

For the last test (5.5 J static), no crack is observed, and the rupture appears suddenly, without a serious stress or strain concentration visible around the damaged area.

As for HO plates, it has been demonstrated that a post-impact crack exists in the vicinity of the impact, even if not easily detectable. But contrary to HO plates, there is no global buckling, and the

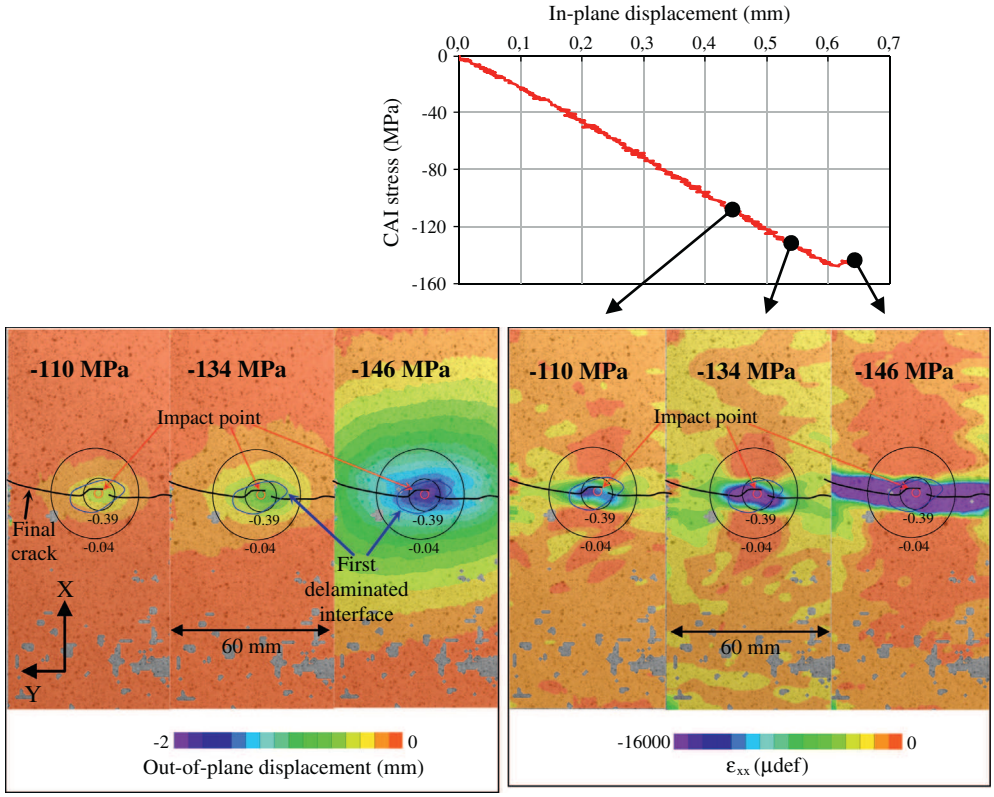


**Fig. 17.** CAI at 29.5 J: stress–displacement curve, out-of-plane displacement field, and longitudinal strain field.

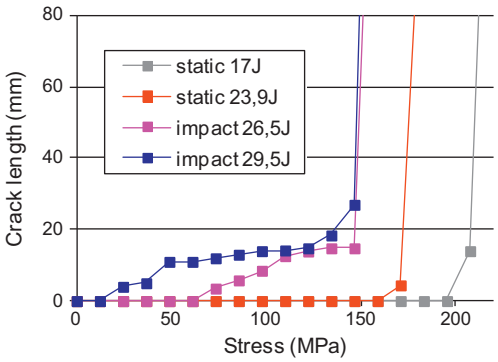


**Fig. 18.** Evolution of crack length during CAI test.

local buckling is quite low. So the propagation of the crack seems not to be driven by buckling, but more by stress concentration around the initial crack due to compression or a combination of compression and bending induced by the local indentation.

Here also the presence of an initial crack and its growth play a major role in the final failure of the plate.

One can wonder if the results obtained in these two specific laminates can be extrapolated to other stacking sequences (0° plies located inside the laminate, thinner plies etc.). Regarding all the observations made in this study, it can be said that as soon as an impact leads to fibre rupture in 0° plies (e.g. initial crack inside the laminate), it is likely to have some stress concentration around the crack, due to compression (pur in-plane loading) or compression and bending combination (if local or global buckling, or local

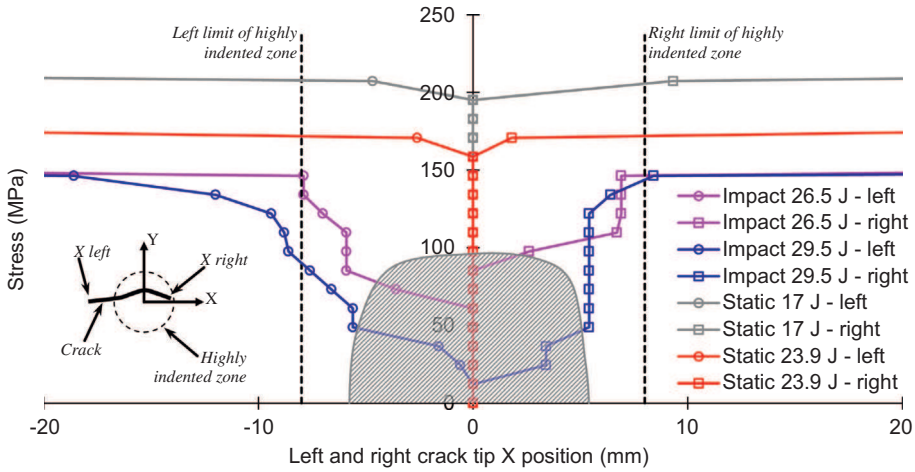


**Fig. 19.** Evolution of left and right crack tips.

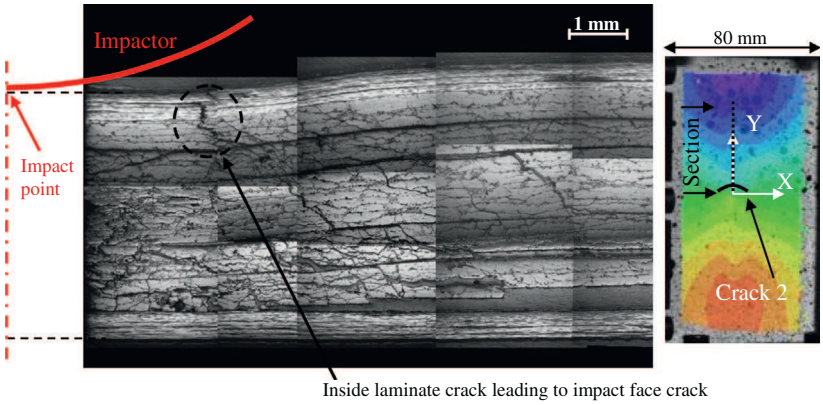


**Fig. 20.** Inside laminate cracks after static indentation.

indentation), resulting in its propagation. The final failure is then very likely to depend on the presence of impact-induced cracks.

## 5. Conclusion

Two different kinds of laminated plates have been tested in compression after impact or static indentation, in order to study the mechanism leading to the failure of the plate. The specimens were initially damaged at a level equivalent or around the BVID, in order to be representative of the damage observed in real composite structures.

For the HO plates, it is clear that the specific damage shape obtained after impact, with the creation of a transverse crack (crack 2) gives a special role to this crack in the failure process. The global buckling imposes the stress field at the crack tip, and drives the propagation of the crack induced by fibre rupture in compression.

For QI tests, the same kind of analysis also shows the propagation of a compression crack during the CAI. This crack is in fact created during the impact, under the impactor. Depending on the level of initial damage, the crack propagation is more or less stable, and happens earlier or later. Like for HO plates, the role of crack is proved to be significant in the final failure, even if the links between buckling and crack propagation is not obvious from a purely experimental analysis.

In any case, failure in plates due to CAI cannot be reduced to a single buckling calculation. This study shows that, in order to have predictive numerical simulations of the residual strength of impacted composite structures, it is necessary to take into account the presence of impact-induced cracks (not only delaminations) and to model crack propagation during CAI loading.

## References


[1] Joint aviation requirements for large aeroplanes (JAR25).
[2] Xiong Y, Poon C. A prediction method for the compressive strength of impact damaged composite laminates. Compos Struct 1995;30:357–67.
[3] Naik NK, Ramasimha R. Estimation of compressive strength of delaminated composites. Compos Struct 2001;52:199–204.
[4] Qi B, Herszbergb I. An engineering approach for predicting residual strength of carbon/epoxy laminates after impact and hygrothermal cycling. Compos Struct 1999;47:483–90.
[5] Suemasu H, Sasaki W, Ishikawa T, Aoki Y. A numerical study on compressive behaviour of composite plates with multiple circular delaminations considering delamination propagation. Compos Sci Technol 2008;68:2562–7.
[6] De Moura MFSF, Gonçalves JPM, Marques AT, De Castro PMST. Modeling compression failure after low velocity impact on laminated composites using interface elements. J Compos Mat 1997;31:1462–79.
[7] Hawyes VJ, Curtis PT, Soutis C. Effect of impact damage on the compressive response of composite laminates. Compos Part A 2001;32:1263–70.
[8] Yan H, Oskay C, Krishnan A, Xu LR. Compression-after-impact response of woven fibre-reinforced composites. Compos Sci Technol 2010;70:2128–36.
[9] González EV, Maimí P, Camanho PP, Turon A, Mayugo JA. Simulation of drop-weight impact and compression after impact tests on composite laminates. Compos Struct 2012;94:3364–78.
[10] Falzon BG, Faggiani A. Predicting low-velocity impact damage in stiffened composite panels using high fidelity finite element modelling. In: 14th European conference on composite materials, Budapest, Hungary; 2010.
[11] Cartie DDR, Irving PE. Effect of resin and fibre properties on impact and compression after impact performance of CFRP. Compos Part A 2002;33:483–93.
[12] Dale M, Acha BA, Carlsson LA. Low velocity impact and compression after impact characterization of woven carbon/vinylester at dry and water saturated conditions. Compos Struct 2012;94:1582–9.
[13] Ishikawa T, Sugimoto S, Matsushima M, Hayashi Y. Some experimental findings in compression-after-impact (CAI) tests of CF/PEEK (APC-2) and conventional CF/epoxy flat plates. Compos Sci Technol 1995;55:349–63.
[14] Duarte A, Herszberg I, Paton R. Impact resistance and tolerance of interleaved tape laminates. Compos Struct 1999;47:753–8.
[15] Lopes CS, Seresta O, Coquet Y, Gürdal Z, Camanho PP, Thuis B. Low-velocity impact damage on dispersed stacking sequence laminates. Part I: Experiments. Compos Sci Technol 2009;69:926–36.
[16] Aymerich F, Priolo P. Characterization of fracture modes in stitched and unstitched cross-ply laminates subjected to low velocity impact and compression after impact loading. Int J Impact Eng 2008;35(7):591–608.
[17] Tan KT, Watanabe N, Iwahori Y, Ishikawa T. Effect of stitch density and stitch thread thickness on compression after impact strength and response of stitched composites. Compos Sci Technol 2012;72:587–98.
[18] Zhang X, Hounslow L, Grassi M. Improvement of low-velocity impact and compression-after-impact performance by z-fibre pinning. Compos Sci Technol 2006;66:2785–94.
[19] Kinsey A, Saunders DEJ, Soutis C. Post-impact compressive behaviour of low temperature curing woven CFRP laminates. Composites 1995;26:661–7.
[20] Aktas M, Karakuzu R, Arman Y. Compression-after impact behaviour of laminated composite plates subjected to low velocity impact in high temperatures. Compos Struct 2009;89:77–82.
[21] Aoki Y, Yamada K, Ishikawa T. Effect of hygrothermal condition on compression after impact strength of CFRP laminates. Compos Sci Technol 2008;68:1376–83.
[22] Berketis K, Tzetzis D, Hogg PJ. The influence of long term water immersion ageing on impact damage behaviour and residual compression strength of glass fibre reinforced polymer (GFRP). Mater Des 2008;29:1300–10.
[23] Qi B, Herszberg I. An engineering approach for predicting residual strength of carbon/epoxy laminates after impact and hygrothermal cycling. Compos Struct 1999;47:483–90.
[24] Uda N, Ono K, Kunoo K. Compression fatigue failure of CFRP laminates with impact damage. Compos Sci Technol 2009;69:2308–14.
[25] Petit S, Bouvet C, Bergeot A, Barrau JJ. Impact and compression after impact experimental study of a composite laminate with cork thermal shield. Compos Sci Technol 2007;67:3286–99.
[26] de Freitas M, Reis L. Failure mechanisms on composite specimens subjected to compression after impact. Compos Struct 1998;42:365–73.
[27] Zhang X, Davies GAO, Hitchings D. Impact damage with compressive preload and post-impact compression of carbon composite plates. Int J Impact Eng 1999;22:485–509.
[28] Habib FA. A new method for evaluating the residual compression strength of composites after impact. Compos Struct 2001;53:309–16.
[29] Wiggenraad JFM, Zhang X, Davies GAO. Impact damage prediction and failure analysis of heavily loaded, blade-stiffened composite wing panels. Compos Struct 1999;45:81–103.
[30] Reis L, de Freitas M. Damage growth analysis of low velocity impacted composite panels. Compos Struct 1997;38:509–15.
[31] Sanchez-Saez S, Barbero E, Zaera R, Navarro C. Compression after impact of thin composite laminates. Compos Sci Technol 2005;65:1911–9.

[32] Ghelli D, Minak G. Low velocity impact and compression after impact tests on thin carbon/epoxy laminates. Compos Part B 2011;42:2067–79.
[33] Khondker OA, Leong KH, Herszberg I, Hamada H. Impact and compression-after-impact performance of weft-knitted glass textile composites. Compos Part A 2005;36:638–48.
[34] Soutis C, Curtis PT. Prediction of the post-impact compressive strength of CFRP laminated composites. Compos Sci Technol 1996;56:677–84.
[35] Airbus Industries Test Method: AITM 1–0010: Determination of compression strength after impact.
[36] Abi Abdallah E, Bouvet C, Rivallant S, Barrau JJ. Experimental analysis of damage creation and permanent indentation on highly oriented plates. Compos Sci Technol 2009;6:1238–45.